Simulation Environment for the Evaluation of 3D Coronary Tree Reconstruction Algorithms in Rotational Angiography.

Guanyu Yang, Alexandre Bousse, Christine Toumoulin, Huazhong Shu

Simulation Environment for the Evaluation of 3D Coronary Tree Reconstruction Algorithms in Rotational Angiography

G. Yang[1,2,3], A. Bousse[1,2,3], C. Toumoulin[2,3] and H. Shu[1,3]

1. Laboratory of Image Science and Technology, Southeast University, Nanjing, 210096, P.R. China

2. INSERM U642, Laboratoire Traitement du Signal et de l'Image, Université de Rennes 1, Rennes, 35042, France

3. Centre de Recherche en Information Biomédicale Sino-français (CRIBS)

***Abstract*— We present a preliminary version of a simulation environment to evaluate the 3D reconstruction algorithms of the coronary arteries in rotational angiography. It includes the construction of a 3D dynamic model of the coronary tree from patient data, the modeling of the rotational angiography acquisition system to simulate different acquisition and gating strategies and the calculation of radiographic projections of the 3D model of coronary tree throughout several cardiac cycles.**

***Index Terms*— Coronary Artery, 3D Reconstruction, Geometric and Physic Models, 3D Rotational Angiography**

I. Introduction

Percutaneous coronary interventions have grown over these last years to become a common revascularization method for the treatment of coronary artery disease.

Even if the traditional biplane X-ray angiography remains the gold standard for both diagnosis and image guided treatment, it has been shown unable to provide reliable geometric information on the lesion (degree of stenosis, length, eccentricity, diameter of the vessel and plaque morphology). It often involves to multiplying the incidences to find the optimal views which will show the lesion clearly while minimizing vessel overlap and foreshortening of vessel segments in areas of interest. The development of the 3D rotational angiography(3D-RA) system brings new perspectives for the 3D reconstruction of the coronary tree. The rotational image acquisition allows the cardiologist to obtain up to 180 projections of the left or right coronary tree during a single injection of contrast under different angles (caudal, cranial, axial). Today, the challenge is to exploit the set of available projections to perform 3D reconstruction of the coronary tree taking into account two kinds of movements: the non linear motion of the structures and the rotation of the acquisition system.

Different techniques are considered for the reconstruction of the coronary tree from projections. A first class relies on 3D modeling techniques either from two views[1] or from selected projections at the same cardiac phase (or rest phase) when considering a rotational acquisition[2]. These methods exploit the epipolar geometry to achieve the 3D reconstruction of coronary tree. A second category used a pre-computed motion model to modify the projection operator and calculate a motion compensated 3D tomographic reconstruction based on ART[3] or filtered back-projection algorithms[4][5]. Nevertheless the quality and the accuracy of the reconstruction need to be objectively evaluated. Different solutions can be considered such as the animal experimentation or the acquisition system modeling and the 3D physical or numerical phantom building.

We propose a simulation environment to evaluate the 3D reconstruction algorithm of the coronary arteries. It includes

- The construction of a 3D dynamic model of the coronary tree from dynamic volumes based on multi-slice computed tomography(MSCT) sequences (volumes reconstructed every 10% of the cardiac cycle). The result is a sequence of volumetric images representing the motion of the coronary arteries throughout the cardiac cycle;
- The modeling of the rotational angiography acquisition system to simulate different acquisition and gating strategies;
- The calculation of radiographic projections of the 3D model of coronary tree throughout several cardiac cycles.

This paper describes a preliminary version of this project: the generation of a geometric coronary tree model (section II), the modeling of the rotational angiography acquisition system and the calculation of projective data from the 3D coronary model (section III). Section IV concludes on the results and gives some perspectives.

II. Coronary Tree Model Generation

A. Source Data

The model described in this paper is based on cardiac MSCT data. Dynamic volume sequences were acquired on a sub second spiral GE 64-slice CT scanner. Each sequence includes 10 volumes reconstructed at every 10% of the R-R interval. The slice thickness is 0.625mm, the pixel size 0.488mm^2 and the size of the isotropic volumes is $512 \times 512 \times 332$.

Although the 64-slice MSCT scanner gives rise to a higher temporal and spatial resolution for the visualization and the assessment of the coronary artery disease, some vascular segments remains not well displayed on several volumes of the sequence because of motion artifacts or severe wall calcification. This makes coronary arteries hard to extract

in these areas. And it is the reason why we focused for a preliminary stage on the generation of a static model from the volume reconstructed at the 80% of the R-R interval.

B. Centerline Extraction

We applied a tracing-based algorithm for the coronary artery central axis extraction[6]. The tracking algorithm relies on a local modeling of the vessel by a cylinder in a 3D homogeneous space. The parameters of this cylinder (location of the center of gravity, and diameter) are estimated using a 3D geometrical moment operator. A multiscale filter based on eigenvalue analysis of the Hessian matrix is then applied to highlight tubular structures and coping with varying widths. It is also used to locally determine the principal direction of the vessel. A detection of possible bifurcation is performed then in the estimated direction. If one bifurcation is detected, more than two seed points are extracted which are saved in a list to be further taken as initial points of the tracking process. The next point P_{i+1} on the centerline is sought out in the estimated direction at the current point P_i by using the moment operator.

C. Region Segmentation

We applied then the watershed algorithm around the extracted centerlines of the vessels to improve the accuracy of the vascular wall delineation. Watershed segmentation considers the regions to be extracted as catchment basins in topography. The idea of watershed is to fill up these basins with water by starting at local minima of gradient map. At the points where water coming from different basins meets, dams are built to constitute the boundaries of the basins or the watershed lines[7].

We performed region segmentation by using the following stages:

1) Define a volume of interest B_i^w around the extracted centerlines. The bottom of the box is centered at each central axis point P_i. The width of this rectangular box is given by the vessel diameter d_i estimated at the previous stage and the length L_i by the span between two points P_i and P_{i+1}. The orientation of the box B_i^w was defined by the local orientation of the vessel $\vec{v}_i^{vessel}$(Fig. 1);
2) Preprocess the volume with a gradient operator inside the B_i^w;
3) Apply 3D watershed algorithm by the Insight Toolkit(ITK) inside the box B_i^w ;
4) Perform 3D region growing starting from the point P_i to extract the vessel according to the label values of P_i.

Watershed algorithm in its original form produces an over-segmentation result of the image. To avoid this problem, watershed depth is introduced to overlook the small basins, which can be defined as the maximum depth of water a catchment basin can hold without flowing into any others[8]. Furthermore, another iterative strategy is performed to alleviate over-segmentation. Given the local vessel in B_i^w is a frustum of a cone, its local volume Vol_i can be calculated

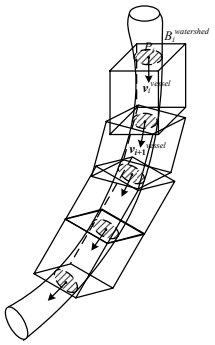

Fig. 1: Watershed algorithm inside a series of interest volumes

by local diameters d_i, d_{i+1} and the distance L_i. Measured by the number of voxels, the calculated local volume Vol_i can be compared with the volume of vessel region, Vol'_i, segmented by watershed algorithm. The ratio γ between these two volumes is thus defined as

$$\gamma = Vol'_i / Vol_i \quad (1)$$

Normally, Vol'_i is larger than Vol_i, which makes γ varying between 1 and 5. If it is less than 1, it suggests that over-segment may take place. The output scale of watershed algorithm will increase by adding a static value until the ratio γ becomes a reasonable one.

Fig. 2 illustrates an extracted 3D coronary tree by 3D watershed method. The aorta was independently segmented with a classical region growing algorithm within a region of interest(ROI).

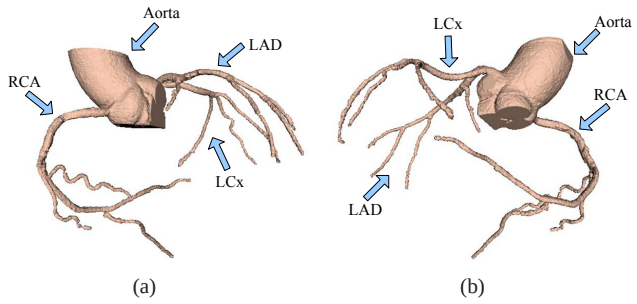

Fig. 2: 3D coronary tree: aorta, left anterior descending artery (LAD), left circumflex branch (LCx) and right coronary artery (RCA) are respectively identified by arrows.

III. 3D Rotational Angiography Simulation

A. System Geometry

The 3D-RA system is composed of an X-ray source and an image intensifier mounted on a motorized computer controlled arc known as the C-arm. The X-ray source is fixed with respect to the center of rotation (ISO Center). The distance source - image plane (*SID*) and the source-ISO Center distance (*ISO*) are two geometric parameters of the system. The entire assembly can rotate along an arc around a table, allowing multiple acquisitions from different angles(Fig. 3). Two angles, named primary angle θ and

secondary angle φ respectively, control the orientation of the C-arm. φ is kept constant over the acquisition time and varies from $-30°$ cranial to $30°$ caudal. θ refers to rotation angle from RAO60° to LAO60° with angular increment (1.5° - 5°) applied during the rotation of the C-arm. Another parameter is available which allows selecting the rotation speed between $30°s^{-1}$ and $40°s^{-1}$.

The size of volume data and its spatial resolution, $N_x^V \times N_y^V \times N_z^V$ and (S_x^V, S_y^V, S_z^V), are provided by source data. Whereas, the size of projection image and its spatial resolution, $N_x^I \times N_y^I$ and (S_x^I, S_y^I), can be specified manually.

After analyzing the geometry of 3D-RA system, volume coordinates and projection image coordinates can be transformed into the system coordinates. Based on the right-hand system coordinates defined in Fig. 3, local volume coordinates $(x, y, z, 1)^T$ and projection image coordinates $(u, v, 0, 1)^T$ can be transformed to the corresponding system coordinates $\left(x_S^V, y_S^V, z_S^V, 1\right)^T$ and $\left(x_S^I, y_S^I, z_S^I, 1\right)^T$ by matrix R_V and R_I respectively. Because the axes of volume coordinates are parallel with the system axes, R_V can be simply defined by scaling and translating.

$$R_V = \begin{bmatrix} S_x^V & 0 & 0 & S_x^V V_x^{Center} \\ 0 & S_y^V & 0 & S_y^V V_y^{Center} \\ 0 & 0 & S_z^V & S_z^V V_z^{Center} \\ 0 & 0 & 0 & 1 \end{bmatrix} \quad (2)$$

where $(V_x^{Center}, V_y^{Center}, V_z^{Center})$ is the user-defined rotation center, which is coincided with the origin of system coordinates, i.e. ISO-Center. Composed of scaling, translation and rotation, R_I can be decomposed into matrix representation as: $R_I = N_I M_I$. N_I represents the 3D rotation transform about an arbitrary unit vector $\vec{u}$ which can obtain by rotating $+z$ axis by φ in yz plane. The detail about N_I calculation can be found in [9]. M_I relating to scaling and translation is defined as

$$M_I = \begin{bmatrix} S_x^I & 0 & 0 & -S_x^I(N_x^I - 1)/2 \\ 0 & S_y^I & 0 & -S_y^I(N_y^I - 1)/2 \\ 0 & 0 & 0 & (SID - ISO) \\ 0 & 0 & 0 & 1 \end{bmatrix} \quad (3)$$

B. Digitally Reconstructed Radiographs

Based on volumetric data reconstructed by CT images, digitally reconstructed radiographs (DRRs) can often be calculated for simulating x-ray projections. A ray-tracing based algorithm was adopted in [10][11] to calculate DRRs based on the transmission principle of x-ray.

The concept of ray-tracing based algorithm is shown in Fig. 4. The ray coming from the x-ray source crosses the volume by intersecting a series of voxels before reaching the image plane. The coordinates of the intersection points P_i^{inter} and the distance d_i^{inter} between each two neighbored points are then calculated in system coordinates. The X-ray energy transmitted through a structure is given by:

$$I = I_0 \sum_{i=1}^{M} e^{-\mu_i d_i^{inter}} \quad (4)$$

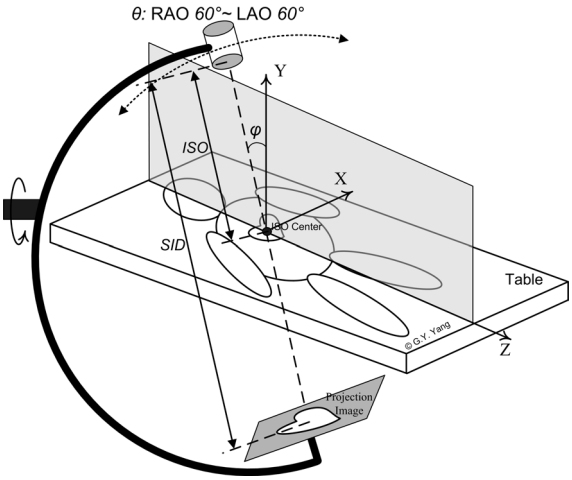

Fig. 3: Geometry of 3D-RA system.

where I_0 is the incident x-ray energy, M is the number of intersection points and μ_i is linear attenuation coefficient for the CT voltage applied during the CT slices acquisition, which can be calculated by CT value of the voxel and the attenuation coefficient of water for the same CT voltage[11].

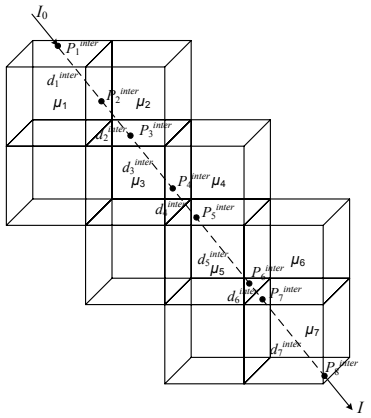

Fig. 4: The concept of DRRs simulation algorithm[11].

During 3D-RA examination, a cardiac catheterization is performed to inject a contrast agent into the arteries in order to improve the contrast between the vessel and the other structures. Fig. 5(a) illustrates one frame of a real cardiac 3D-RA sequence with size 1024×1024 and $0.13 mm^2$ spatial resolution, in which left coronary artery (LCA) filled with contrast agent is shown with lower intensity than the background. Considering the reality of simulation, two volumes, the raw intensity volume and binary volume of segmented vessel, are employed in the simulation. The binary volume, marking the region of interested vessel, serves as a mask in the raw intensity volume data to simulate the projections of the vessel tree with contrast agent. In detail, within the marked vessel region, high attenuation coefficient μ_i^V is adopted to attenuate the energy of x-ray greatly for simulating contrast agent. Otherwise, low attenuation

coefficient μ_i^B is selected to generate the background. The attenuation coefficient can be defined by

$$\begin{cases} \mu_i^V = a\mu_i + b, \text{ voxel belongs to the vessel region} \\ \mu_i^B = a\mu_i, \text{ else} \end{cases} \quad (5)$$

where a is specified less than 1 to decrease the μ_i and b increases μ_i of the voxels in the vessel region. In particular, we defined a, b equal to 0.1 and 0.2 respectively.

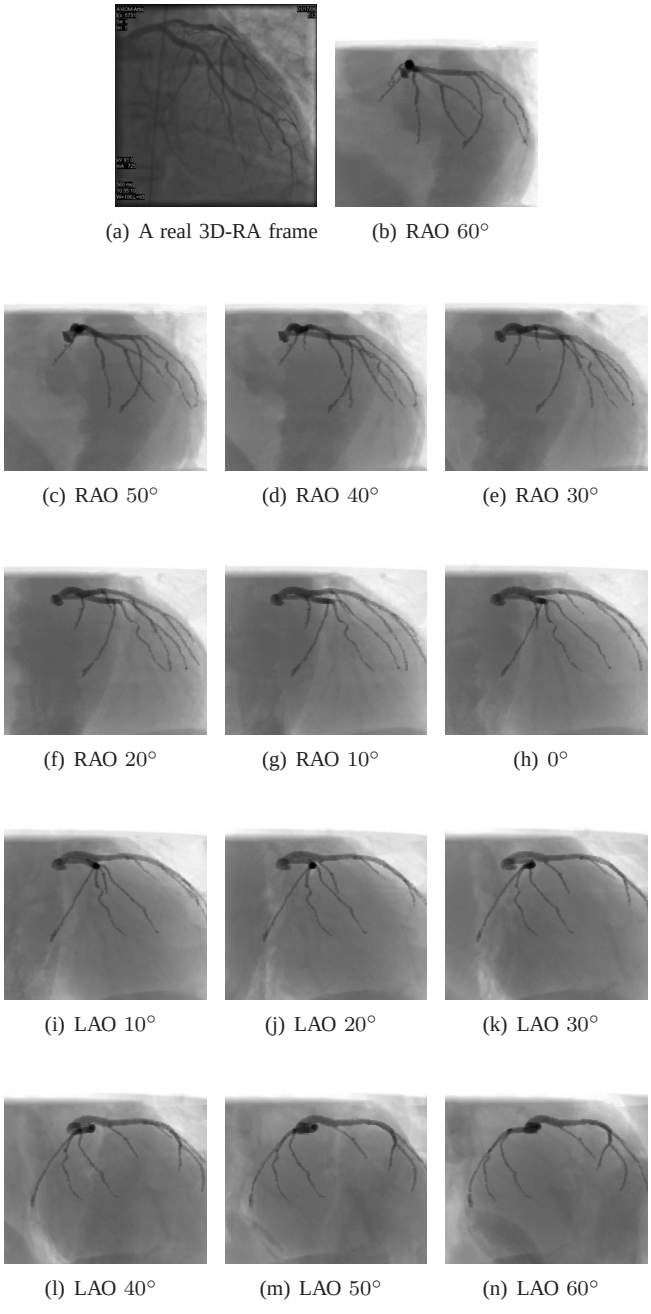

(a) A real 3D-RA frame (b) RAO 60° (c) RAO 50° (d) RAO 40° (e) RAO 30° (f) RAO 20° (g) RAO 10° (h) 0° (i) LAO 10° (j) LAO 20° (k) LAO 30° (l) LAO 40° (m) LAO 50° (n) LAO 60°

Fig. 5: (a): A frame of real 3D-RA sequence of LCA, (b)-(n): 3D-RA simulation of LCA in source data.

C. Simulation Results

In Fig. 5 (b) to (n), thirteen simulated projections of LCA in 3D artery model of Fig. 2 are picked out each $10°$ from RAO $60°$ to LAO $60°$. Due to the high computation complexity, the size of volume was decreased to a lower one, $256 \times 256 \times 200$ with 0.66mm^3 spatial resolution. According to the size of LCA, the simulated projection images were specified to be 330×330 pixels with 0.4mm^2 isotropic spatial resolution. In the simulated projections, the skeletons of coronary arteries were illustrated with similar image backgrounds. But the spatial resolution of volume with at most 0.33mm^3 limited the resolution of simulated projections greatly. In addition, the manner of contrast agent injection makes the difference between simulated and real images. In the cardiac MSCT the blood with contrast agent flowed all over the body, while, in 3D-RA the contrast agent congregated in the interested branches at the imaging moment. As a result, the background of 3D-RA typically composed of vertebral column, costal bones and lung was blurred with cardiac cavities, aorta and pulmonary arteries in the simulated projections.

IV. Conclusion

In this paper, we have described a preliminary version of a simulated environment to evaluate the 3D reconstruction algorithm of moving structures in X-ray rotational angiography. This version performs a rotational acquisition of a static object. We are currently working on the construction of the 3D dynamic model of the coronary tree to be able to simulate the acquisition of a moving structure.

References

[1] S. J. Chen and J. D. Carroll, "3-D reconstruction of coronary arterial tree to optimize angiographic visualization," *Medical Imaging, IEEE Transactions on*, vol. 19, no. 4, pp. 318–336, 2000.

[2] B. Movassaghi, V. Rasche, M. A. Viergever, and W. J. Niessen, "3D coronary reconstruction from calibrated motion-compensated 2D projections based on semi-automated feature point detection," *Proceedings of SPIE*, vol. 5370, pp. 1943–1950, 2004.

[3] C. Blondel, G. Malandain, R. Vaillant, and N. Ayache, "Reconstruction of coronary arteries from a single rotational X-ray projection sequence," *Medical Imaging, IEEE Transactions on*, vol. 25, no. 5, pp. 653–663, 2006.

[4] D. Schäfer, J. Borgert, V. Rasche, and M. Grass, "Motion-compensated and gated cone beam filtered back-projection for 3-D rotational X-ray angiography," *Medical Imaging, IEEE Transactions on*, vol. 25, no. 7, pp. 898–906, 2006.

[5] S. Bonnet, A. Koenig, S. Roux, P. Hugonnard, R. Guillemaud, and P. Grangeat, "Dynamic X-ray computed tomography," *Proceedings of the IEEE*, vol. 91, no. 10, pp. 1574–1587, 2003.

[6] G. Yang, A. Bousse, C. Toumoulin, and H. Shu, "A multiscale tracking algorithm for the coronary extraction in msct angiography," *Engineering in Medicine and Biology Society, 2006. EMBS '06. 28th Annual International Conference of the IEEE*, pp. 3066–3069, 2006.

[7] J. B. T. M. Roerdink and A. Meijster, "The Watershed Transform: Definitions, Algorithms and Parallelization Strategies," *Fundamenta Informaticae*, vol. 41, no. 1-2, pp. 187–228, 2001.

[8] L. Ibáñez, W. Schroeder, L. Ng, and J. Cates, "The ITK Software Guide, Kitware," *Inc., http://www. itk. org*, 2005.

[9] F. S. Hill, *Computer Graphics Using Open GL (2nd Edition)*. Prentice Hall, 2000.

[10] G. W. Sherouse, K. Novins, and C. E. L., "Computation of digitally reconstructed radiographs for use in radiotherapy treatment design," *International journal of radiation oncology, biology, physics*, vol. 18, no. 3, pp. 651–658, 1990.

[11] N. Milickovic, D. Baltas, S. Giannouli, M. Lahanas, and N. Zamboglou, "CT imaging based digitally reconstructed radiographs and their application in brachytherapy," *Physics in Medicine & Biology*, vol. 45, no. 10, pp. 2787–2800, 2000.